

# Interplay of local moment and itinerant magnetism in cobalt-based Heusler ferromagnets: $\text{Co}_2\text{TiSi}$ , $\text{Co}_2\text{MnSi}$ and $\text{Co}_2\text{FeSi}$

Guanhua Qin,<sup>1,2,3</sup> Wei Ren<sup>1,3,\*</sup> and David J. Singh<sup>2,4,†</sup><sup>1</sup>State Key Laboratory of Advanced Special Steel, Shanghai Key Laboratory of Advanced Ferrometallurgy and Physics Department, Shanghai University, Shanghai 200444, China<sup>2</sup>Department of Physics and Astronomy, University of Missouri, Columbia, Missouri 65211-7010, USA<sup>3</sup>Shanghai Key Laboratory of High Temperature Superconductors, MGI and ICQMS, Shanghai University, Shanghai 200444, China<sup>4</sup>Department of Chemistry, University of Missouri, Columbia, Missouri 65211, USA

(Received 29 July 2019; revised manuscript received 10 November 2019; published 21 January 2020)

Heusler ferromagnets based on Co are important materials for spintronics. This is due to the exceptional combinations of high Curie temperature and strong spin polarization, including half-metallicity, found in some of these. We investigate the full Heusler compounds,  $\text{Co}_2\text{TiSi}$ ,  $\text{Co}_2\text{MnSi}$ , and  $\text{Co}_2\text{FeSi}$  using first principles calculations.  $\text{Co}_2\text{TiSi}$  and  $\text{Co}_2\text{MnSi}$  are half metals, while  $\text{Co}_2\text{FeSi}$  is not. The trends in the Curie temperatures are reproduced by the calculated spin wave dispersions. Remarkably,  $\text{Co}_2\text{TiSi}$  is a very itinerant magnet but  $\text{Co}_2\text{FeSi}$  and  $\text{Co}_2\text{MnSi}$  show local moment behavior regarding the Fe and Mn, while retaining the itinerancy of the Co magnetism. These materials can therefore be described as itinerant systems with embedded local moment atoms. This provides an explanation for their exceptional behavior. Our results do not support the half-metallic character proposed for  $\text{Co}_2\text{FeSi}$ , but they are consistent with a higher Curie temperature relative to the Mn compound. The density of states and transport spin polarizations  $\text{Co}_2\text{FeSi}$  have opposite signs. Importantly, although there is a large minority spin density of states at the Fermi level, leading to a low density of states spin polarization, we find a very strong transport spin polarization in  $\text{Co}_2\text{FeSi}$ . This, combined with the large moment, cubic structure, and high Curie temperature supports the further investigation of  $\text{Co}_2\text{FeSi}$  for spintronic applications that make use of the transport spin polarization.

DOI: [10.1103/PhysRevB.101.014427](https://doi.org/10.1103/PhysRevB.101.014427)

## I. INTRODUCTION

Magnetic materials applicable to spintronics is a topic of strong interest. Cobalt and cobalt-based intermetallics are important magnetic materials and are useful in technologies. This includes elemental cobalt, which is a high temperature ferromagnet with substantially itinerant character, Sm-Co hard magnets, such as  $\text{SmCo}_5$ , and  $\text{Sm}_2\text{Co}_{17}$  [1], as well as compounds showing weakly magnetic character as in pnictide superconductor related alloys ( $\text{BaFe}_{2-x}\text{Co}_x\text{As}_2$  and  $\text{BaCo}_2\text{As}_2$ ) [2]. The full Heusler ferromagnets,  $\text{Co}_2\text{TiSi}$ ,  $\text{Co}_2\text{MnSi}$ , and  $\text{Co}_2\text{FeSi}$  are remarkable from this perspective. These materials have been extensively investigated as potential half metals [3–17], and furthermore  $\text{Co}_2\text{MnSi}$  and  $\text{Co}_2\text{FeSi}$  show remarkably high Curie temperatures  $T_C$ . In the case of  $\text{Co}_2\text{FeSi}$ , the reported Curie temperature is as high as 1100 K [3,4]. This suggests use in spintronic applications. However, as discussed below, the properties of  $\text{Co}_2\text{FeSi}$  in particular have been controversial, with the material having different reported Curie temperatures and being reported as half metallic, ideal for spintronics, or not.

The high Curie temperature of  $\text{Co}_2\text{FeSi}$  has been discussed in literature in terms of a generalized Slater-Pauling

rule in which the magnetic moment is understood in terms of electron count and  $T_C$  depends linearly on the magnetic moment [18]. Estimates of the Curie temperature based on spin-wave dispersions from spin spiral calculations support this high Curie temperature [19]. However, there are also literature reports of lower Curie temperatures,  $T_C \sim 980$  K, and lower magnetizations in  $\text{Co}_2\text{FeSi}$  [20,21].  $\text{Co}_2\text{TiSi}$ , which contains nonmagnetic Ti, has  $T_C = 380$  K, while  $\text{Co}_2\text{MnSi}$  has  $T_C = 985$  K [20,22–24].

The present paper examines these issues from the point of view of density functional calculations and provides a view of these materials as having a high Curie temperature and other magnetic properties controlled by the interplay of local moments associated with Fe and Mn that are embedded in an itinerant ferromagnetic background associated with the Co, as exemplified by  $\text{Co}_2\text{TiSi}$ . We also find that while  $\text{Co}_2\text{FeSi}$  is not half metallic and is not close to being half metallic from a density of states point of view, it does have a high transport spin polarization. This may enable some types of spintronic devices based on it, while at the same time making it unsuitable for other devices that depend on tunneling.

## II. METHODS

The results reported here were obtained within density functional theory (DFT) using the Perdew-Burke-Ernzerhof generalized gradient approximation (PBE GGA) [25], except

\*renwei@shu.edu.cn

†singhdj@missouri.edu

as noted. The calculations were done using the general potential linearized augmented plane-wave method [26], as implemented in the WIEN2K and ELK codes [27,28]. We checked these two codes for consistency and find no significant differences for these materials. The reported calculations are done at the experimental lattice parameters of 5.733 Å, for Co<sub>2</sub>TiSi, 5.645 Å, for Co<sub>2</sub>MnSi and 5.640 Å, for Co<sub>2</sub>FeSi. The relaxed lattice parameters are very similar to these, specifically, 5.747 Å, 5.626 Å, and 5.632 Å, for Co<sub>2</sub>TiSi, Co<sub>2</sub>MnSi, and Co<sub>2</sub>FeSi, respectively. The close agreement of the lattice parameters supports the validity of the method used.

We note that there are prior calculations, based on the DFT+*U* methodology [29]. In those calculations it was found that adding *U* could lead to half-metallic ferromagnetism in Co<sub>2</sub>FeSi for a certain range of the effective Hubbard interaction,  $U_{\text{eff}}$  in the range between 2 eV and 5 eV, but that values of  $U_{\text{eff}}$  of 2 eV or higher then leads to destruction of the experimentally observed half-metallic state in Co<sub>2</sub>MnSi. Furthermore, as discussed below, the Co in these materials behaves very much as an itinerant system, similar to elemental Co. It has been shown that the use of DFT+*U* for such itinerant transition metals, including Fe and Co, leads to results in extremely poor agreement with experiment, even if first principles derived linear response values of  $U_{\text{eff}}$  are employed [30,31]. In fact PBE provides a much better description than higher level methods such as hybrid functionals, for these materials [31]. This is not to say that DFT+*U* is inferior to standard DFT for localized systems, such as many transition metal oxides.

Very recently, Nawa and Miura have proposed a mixed scheme where they apply DFT+*U* only to some transition element sites, particularly Fe and Mn in full-Heusler materials [32]. However, in bcc Fe, which shows more local moment behavior than Co [33,34], similar to the Fe in the full-Heuslers, DFT+*U* calculations yield very poor agreement with experiment [31]. Furthermore, it might be expected from the fact that Co is to the right of Fe and Mn in the periodic table that Co should have larger or at least similar *U* to Fe and Mn. This is the case according to reported constrained density functional theory calculations of *U* for Co<sub>2</sub>MnSi and Co<sub>2</sub>FeSi [35]. It is not clear at this time if the mixed approach yields results in better accord with experiment for full-Heusler compounds. It is also noteworthy that GW calculations have been reported for Co<sub>2</sub>FeSi that find good agreement with reported spectroscopic measurements similar to standard Kohn-Sham approaches but with an enhancement of the magnetization [8].

Spin excitations were calculated within the framework of time dependent density functional theory (TDDFT), using the ELK code. Within TDDFT the magnon dispersions can be obtained from the transverse response function  $\chi^+(\mathbf{q}, \omega)$ . This is determined by a Dyson-like [36] equation [37–39],

$$\chi = \chi_0 + \chi_0(1 + f_{xc})\chi, \quad (1)$$

where  $\chi$  is the physical (enhanced) susceptibility of the system, and  $f_{xc}$  is the exchange-correlation kernel, which is a functional derivative of the exchange-correlation potential. In this equation,  $\chi_0$  is the bare Kohn-Sham susceptibility. Here we used the adiabatic local density approximation (ALDA) for  $f_{xc}$ . The zone integration for these response calculations

was done using a uniform 20×20×20 **k**-point mesh in the Brillouin zone.

	$M_{\text{spin}}$ ( $\mu_B$ )	$M_{\text{Co}}$ ( $\mu_B$ )	$M_B$ ( $\mu_B$ )	$E_{\text{mag}}$ (eV)	$N(E_F)$ ( $\text{eV}^{-1}$ )
Co <sub>2</sub> TiSi	2.00	1.02	0.00	0.19	0.97
Co <sub>2</sub> MnSi	5.00	1.06	3.00	1.59	0.77
Co <sub>2</sub> FeSi	5.52	1.38	2.84	1.36	3.32

was done using a uniform 20×20×20 **k**-point mesh in the Brillouin zone.

### III. RESULTS AND DISCUSSION

We begin with the electronic structures. Co<sub>2</sub>TiSi and Co<sub>2</sub>MnSi are found to be half metals with integer spin moments of 2  $\mu_B/\text{f.u.}$  and 5  $\mu_B/\text{f.u.}$ , respectively. This is in accord with experiment and prior theoretical work [6,19,22,23]. We do not obtain a half-metallic state for Co<sub>2</sub>FeSi. The calculated spin moment is 5.52  $\mu_B/\text{f.u.}$  Basic magnetic properties of the three compounds are summarized in Table I. The individual moments, as given by the integrated spin moments in the corresponding LAPW spheres, are also shown. As seen, the Co spin moments for half-metallic Co<sub>2</sub>TiSi and Co<sub>2</sub>MnSi are similar, while the value for Co<sub>2</sub>FeSi is larger, indicating a difference in electronic structure.

The band structures of ferromagnetic Co<sub>2</sub>TiSi, Co<sub>2</sub>MnSi, and Co<sub>2</sub>FeSi are shown in Fig. 1, along with the corresponding electronic densities of states. These electronic structures are similar to those reported previously [7,19,22,23,40]. Both Co<sub>2</sub>TiSi and Co<sub>2</sub>MnSi show gaps in the minority spin leading to half-metallic behavior, while Co<sub>2</sub>FeSi does not have such a gap and is not a half metal according to these calculations. This is also evident from the noninteger spin magnetization, as mentioned above. Importantly, there is a dispersive minority spin band that dips below the Fermi level  $E_F$  at the *X* point in Co<sub>2</sub>FeSi. This extends to  $\sim -0.6$  eV, relative to  $E_F$ , and almost touches the next lower minority band at *X*. This makes it impossible for small changes to lead to half-metallic behavior.

Thus transport in both spin channels is expected for Co<sub>2</sub>FeSi. However, we find a very strong spin polarization for transport even though the density of states in the minority spin is substantial. This means that even though it is not a half metal according to our calculations, Co<sub>2</sub>FeSi may nonetheless be a useful material for spintronics especially considering its cubic structure and high Curie temperature. Furthermore the density of states and transport spin polarization are opposite. This is an interesting case because experiments in between the diffusive and tunneling regimes may then measure particularly low spin polarization, while more ideal devices in the diffusive regime may be able to exploit the high transport spin polarization.

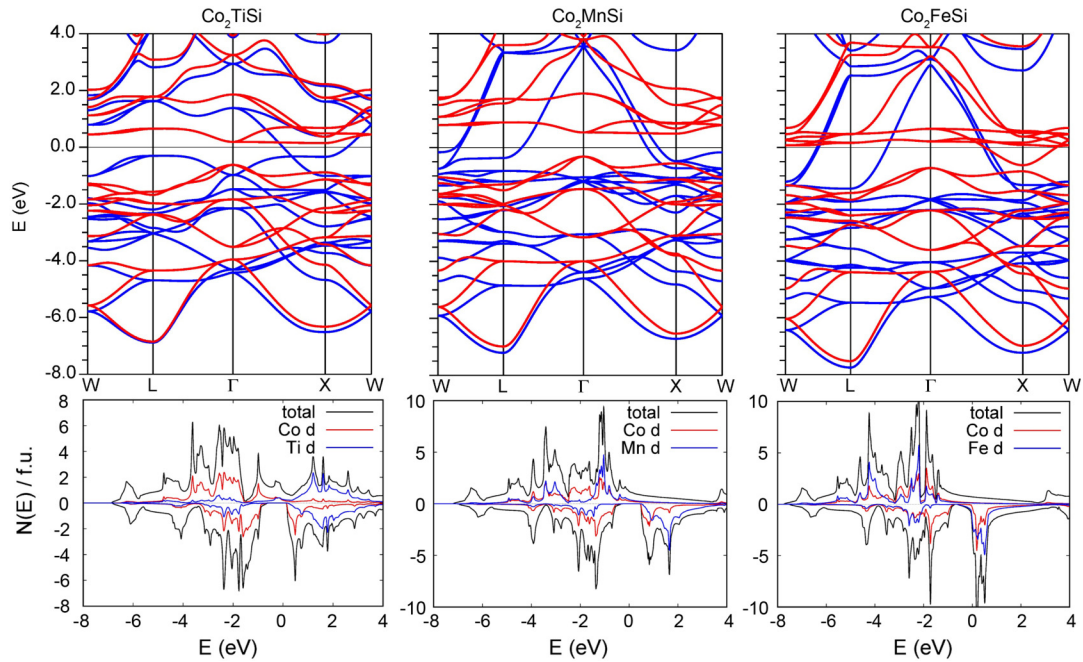


FIG. 1. Calculated band structures of the  $\text{Co}_2\text{BSi}$  compounds (top). Majority spin bands are shown in blue and minority spin in red. Note that all three compounds have very dispersive majority spin bands (blue) crossing the Fermi level, and much less dispersive minority spin bands (red) just above the Fermi level  $E_F$ . Electronic densities of states are in the bottom panels. Majority spin is shown as positive and minority spin is negative. Projections are of  $d$  character in the corresponding LAPW spheres of radii 2.3 Bohr and 1.8 Bohr, for the metal and Si atoms, respectively.

This rather unusual situation where one has high transport spin polarization and low opposite sign density of states spin polarization is due to the specific band structure of the material. The majority and minority spin Fermi surfaces responsible for this are shown in Fig. 2. The majority spin shows two large sheets of Fermi surface, with a nearly spherical shape. The minority spin shows two sheets: one flattened sheet at the  $X$  point of the Brillouin zone and a small section at the  $K$  point (the center of the connection between two  $W$  points). As seen in Fig. 1, the minority spin Fermi surface originates in much less dispersive bands than the majority spin Fermi surface. This is also evident in the density of states of Fig. 1. The Fermi level occurs in a flat region of density of states for the majority spin, characteristic of wide bands, while the minority spin is at the onset of a relatively narrow peak in the density of states derived from Co  $d$  and Fe  $d$  states.

The spin polarization for quantity  $f$  is defined as

$$P_f = \frac{f_{\uparrow} - f_{\downarrow}}{f_{\uparrow} + f_{\downarrow}}. \quad (2)$$

Here  $f$  can be the conductivity  $\sigma$  to produce the transport spin polarization  $P_{\sigma}$ , the density of states  $D = N(E_F)$ , for the density of states spin polarization  $P_D$  or other quantities.

We did transport calculations based on the calculated electronic structure using the BoltzTraP code [41]. This code yields the transport integral for the conductivity,  $\sigma$  modulo, an undetermined scattering time  $\tau$ . The value quoted is from calculations at 50 K, but there is very little temperature dependence. The value of the transport spin polarization at 300 K is only 2% smaller. The obtained value of  $\sigma/\tau$  is proportional to the product of electronic density of states

$N(E_F)$  and average Fermi velocity,  $\langle v_F^2 \rangle$  at low temperature. In a parabolic band model with fixed number of carriers the resulting  $\sigma/\tau$  is inversely proportional to the effective mass

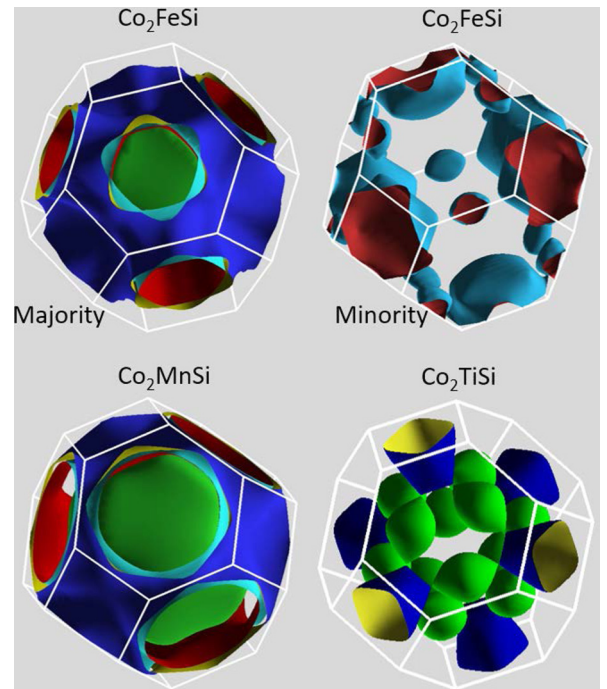


FIG. 2. Majority (top, left) and minority spin (top, right) Fermi surface of  $\text{Co}_2\text{FeSi}$ . Along with the majority spin Fermi surfaces of half-metallic  $\text{Co}_2\text{MnSi}$  (bottom, left) and  $\text{Co}_2\text{TiSi}$  (bottom, right).

TABLE II. Electronic properties at the Fermi energy.  $N(E_F)$  is given in  $\text{eV}^{-1}$  per formula unit and  $\sigma/\tau$  is given in  $10^{21} (\Omega\text{ms})^{-1}$ .

	$N(E_F)_\uparrow$	$N(E_F)_\downarrow$	$P_D$	$(\sigma/\tau)_\uparrow$	$(\sigma/\tau)_\downarrow$	$P_\sigma$
$\text{Co}_2\text{TiSi}$	0.97	0.00	1.00	0.31	0.00	1.00
$\text{Co}_2\text{MnSi}$	0.77	0.00	1.00	0.82	0.00	1.00
$\text{Co}_2\text{FeSi}$	0.71	2.61	-0.57	1.46	0.10	0.87

$m^*$ , reflecting the fact that although they lead to high density of states flat bands are unfavorable for transport.

In any case,  $\sigma/\tau$  is sufficient to calculate the transport spin polarization with the assumption that the scattering time is the same for the two spin channels. This assumption has been applied to complex magnetic systems, for example,  $\text{SrRuO}_3$ , where a reasonable description of experimental data is found. This includes predictions, as in  $\text{SrRuO}_3$ , where an unexpected transport spin polarization opposite to the magnetization was predicted and then found experimentally [42–44]. In general, the scattering mechanisms can have spin dependence and in general this depends on sample details. Nonetheless in a high spin polarization material such as we find for  $\text{Co}_2\text{FeSi}$  this is unlikely to lower the spin polarization strongly, and furthermore in  $\text{Co}_2\text{FeSi}$  the density of states is higher in the minority spin channel, which would suggest if anything a lower  $\tau$  for that spin channel with an enhancement of the already high transport spin polarization.

As seen in Table II, the density of states spin polarization of  $\text{Co}_2\text{FeSi}$  is modest and negative. However, the transport spin polarization is very high. Additionally, it is interesting to observe that it is positive, in other words that it has opposite sign to the density of states spin polarization. Returning to the electronic structure, it may be noted that the minority spin gap in the parent compound,  $\text{Co}_2\text{TiSi}$ , is between groups of Co  $d$  derived bands with relatively high density of states reflecting relatively flat dispersion (note here we refer to  $\text{Co}_2\text{TiSi}$  as the parent, because Ti is nonmagnetic and the other compounds have magnetic atoms on the Ti site). On the other hand, the Fermi level lies in a lower density of states region for the majority spin which has substantial nontransition metal (Si) character. The corresponding bands are considerably more dispersive as is evident in the band structure. In the cases of  $\text{Co}_2\text{MnSi}$  and  $\text{Co}_2\text{FeSi}$  the Fermi level lies above the  $d$  bands for majority spin, i.e., it is in a region of broad Si derived bands with little  $d$  character. This is similar to the band character of  $\text{NiSi}$ , which is an electrode material with a remarkably high conductivity [45–47]. On the other hand, the minority spin Fermi level lies in a region of  $d$  bands, in particular in a gap between  $d$  bands for  $\text{Co}_2\text{MnSi}$  and in the lower part of a  $d$  band peak  $\text{Co}_2\text{FeSi}$ .

Magnetic tunnel junctions have been fabricated using  $\text{Co}_2\text{FeSi}$  by Gersci and co-workers [9]. The magnetoresistance in this type of device is governed by the density of states spin-polarization  $P_D$  [48–50], although there is also a dependence on the nature of the interfaces and tunneling probabilities that may depend on details of the band structure. This is discussed in detail in Ref. [50]. In any case, Gersci and co-workers obtained a value of the spin polarization  $P = 0.50$  from these measurements. This is close in magni-

tude to the value of  $P_D = -0.57$  from our band calculations. One may note that  $P$  occurs in products in the Julliere formula [48–50],

$$TMR = 2P_1P_2/(1 - P_1P_2), \quad (3)$$

where the tunneling magnetoresistance  $TMR$  is controlled by the spin polarization of the density of states polarization at the Fermi level of the two materials,  $P_1$  and  $P_2$ , so that the absolute sign may be difficult to determine.

Point contact Andreev reflection (PCAR) measurements were reported on different samples [9,12]. In this method a superconducting tip is brought into contact with the sample and the Andreev reflection is measured using the dependence of the conductivity on bias voltage [51–53]. These studies yielded PCAR polarizations in the range 48% to 59%. The PCAR spin polarization is equal to the transport spin polarization in the case where there is strong scattering in the sample, i.e., in the diffusive limit. However, these measurements require a junction with a superconducting material and therefore must be done at low temperature, where the transport may be intermediate between diffusive and ballistic. In the ballistic regime the transport is governed by states weighted by the band velocity in the direction of transport, rather than the square of the band velocity. This introduces both geometry and sample dependence [51–55]. Nonetheless those measurements are indicative of sizable spin polarization, but are inconsistent with true half-metallic behavior.

We also did calculations including spin-orbit coupling to check whether orbital moments could explain the difference between the spin magnetization and the reported low temperature magnetization as reported by Wurmehl and co-workers [3,4]. We find orbital moments parallel to the spin moments, as expected based on Hund’s third rule for a more than half full shell. However, the values are  $m_{\text{orb}} = 0.040 \mu_B$  for Co and  $m_{\text{orb}} = 0.067 \mu_B$  for Fe, for a total orbital moment of  $0.147 \mu_B$  per formula unit. This is far too small to explain the discrepancy.

An interesting puzzle is then the high Curie temperature. This was explained using an itinerant Slater-Pauling relation. The explanation is based on half metallicity and a linear connection between the magnetization and the Curie temperature [18]. However, we do not find half metallicity and this is consistent with other recent calculations and several experiments. Within this picture,  $\text{Co}_2\text{FeSi}$  might be expected to have significantly lower Curie temperatures if the magnetization were lower than the half-metallic value. On the other hand, the strong experimental evidence of finite spin polarization is difficult to reconcile with a half-metallic state and therefore with a spin magnetization of  $6 \mu_B$  per formula unit. We therefore compare the spin excitations of  $\text{Co}_2\text{MnSi}$  and  $\text{Co}_2\text{FeSi}$ , using density functional calculations. These calculations do not produce a half-metallic state and therefore address the question of whether the high Curie temperature is linked to half metallicity. The result of these TDDFT calculations is shown in Fig. 3. Cuts at different  $\mathbf{k}$  points along  $\Gamma$ - $X$  are shown in Fig. 4. As seen, the spin excitations of  $\text{Co}_2\text{TiSi}$  become incoherent away from the zone center. This is a consequence of the itinerant nature of the material and especially transitions to minority spin states just above the Fermi level as seen in the band structure. It should also be noted from Fig. 4

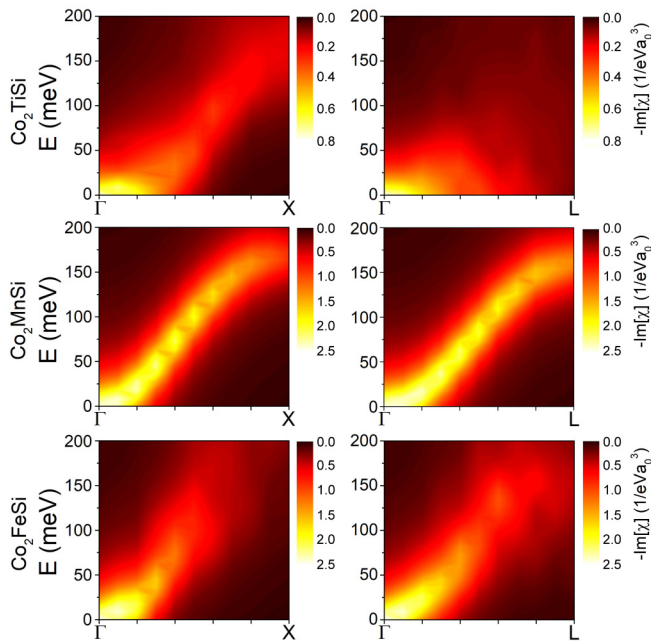


FIG. 3. Spin excitations plotted as the imaginary part of the susceptibility from TDDFT calculations. The left panels show the  $\Gamma$ -X direction, while the right panels show  $\Gamma$ -L.

that there are additional small broad peaks in the imaginary susceptibility at energies above the lowest magnon branch, especially towards the zone boundary in  $\text{Co}_2\text{TiSi}$  and  $\text{Co}_2\text{FeSi}$ . In a local moment Heisenberg picture, with three magnetic atoms per unit cell, three magnon branches may be expected, while with two magnetic atoms per cell, as in  $\text{Co}_2\text{TiSi}$ , two branches may be expected. In itinerant materials, the spectral function reflects electronic excitations, and can have different numbers of peaks, often with considerable damping. The present materials show complex behavior with low amplitude broad peaks at higher energy, reflecting the itinerant nature of the magnetism.

One notes that the energy scales for  $\text{Co}_2\text{MnSi}$  and  $\text{Co}_2\text{FeSi}$  are similar, but that  $\text{Co}_2\text{FeSi}$  has a higher stiffness near  $\Gamma$ . A fit of the spin wave dispersion to a quadratic form appropriate for a ferromagnet yields a coefficient  $D = 197 \text{ meV } \text{\AA}^2$  for  $\text{Co}_2\text{MnSi}$  and  $D = 222 \text{ meV } \text{\AA}^2$  for  $\text{Co}_2\text{FeSi}$ . This is consistent with a  $\sim 15\%$  higher Curie temperature in the Fe compound, although it is not a half metal. A similar fit for  $\text{Co}_2\text{TiSi}$  yields a much smaller  $D = 86 \text{ meV } \text{\AA}^2$ , consistent with its much lower Curie temperature.

Magnetic materials are often classified according to the extent to which they are itinerant or local moment in nature [56–58]. In the local moment limit, stable moments are present on the ions due to intra-atomic interactions. These are subject to intersite interactions that provide the magnetism through ordering of the moments. Local moment magnets can often be described by the Heisenberg or related spin models. The opposite, itinerant limit, is exemplified by materials such as  $\text{ZrZn}_2$ , and to a lesser extent elemental Ni and Co [57]. In this limit, there are not stable moments, but instead ordering arises from conduction electrons, and in fact magnetic states may not even exist for some ordering patterns. This is seen

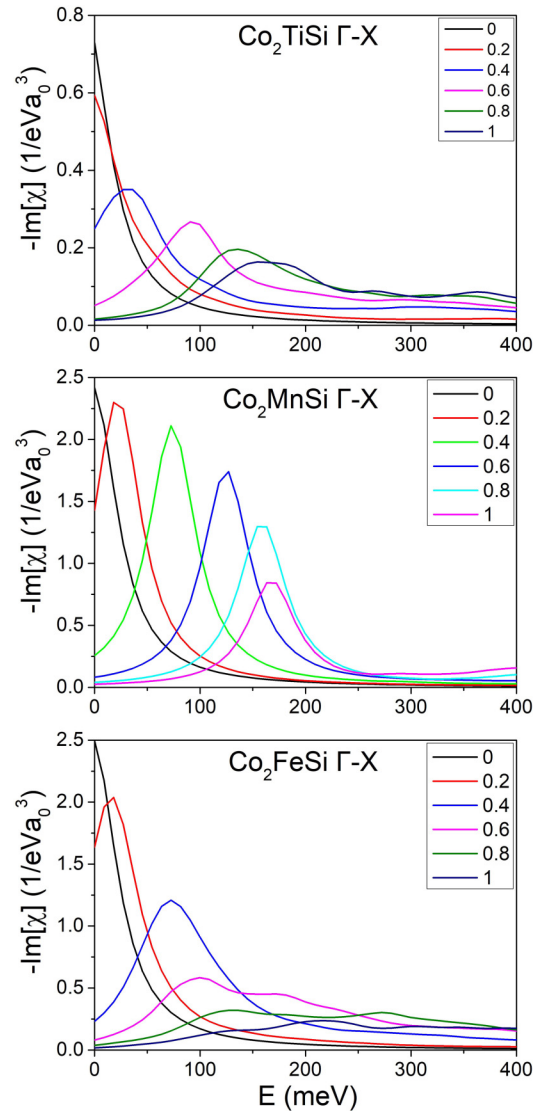


FIG. 4. Energy dependent imaginary susceptibilities for different crystal momenta, along  $\Gamma$ -X, where 0 corresponds to  $\Gamma$  and 1 corresponds to X.

for example from merging of spin-wave excitations seen by neutron scattering into a Stoner continuum at high wave vectors [59]. This can lead to very high ordering temperatures, such as the very high Neel temperature found in  $\text{SrTcO}_3$  [60]. Both of these types of magnetism can be described by DFT calculations, as exemplified by work on  $\text{BaMn}_2\text{As}_2$ ,  $\text{Y}_2\text{Ni}_7$  and other materials [61–64]. The Slater-Pauling curve that was used to understand the Curie temperatures of Heusler compounds is based on an itinerant framework. In order to address the issue of the magnetic nature of these compounds we did calculations including fixed spin moment calculations [65,66].

We begin with  $\text{Co}_2\text{TiSi}$ . This may be regarded as the parent compound of  $\text{Co}_2\text{MnSi}$  and  $\text{Co}_2\text{FeSi}$ , where the magnetic Mn or Fe atom is replaced by the magnetically inert element Ti. The connection between the three compounds is emphasized by the similar structures in the electronic densities of states for the Co sites (lower panels of Fig. 1), although the Fermi

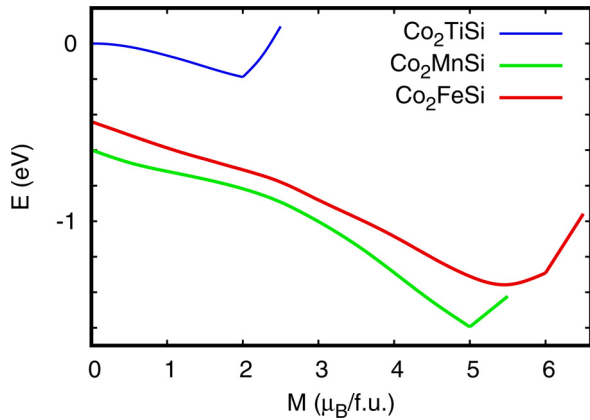


FIG. 5. Fixed spin moment energy as a function of magnetization. The energy zero is taken as the energy of a non-spin-polarized calculation. Note that for  $\text{Co}_2\text{MnSi}$  and  $\text{Co}_2\text{FeSi}$  the zero moment solution has opposite Co and Mn or Fe moments, and an energy below the non-spin-polarized solution. Energies and magnetizations are per formula unit.

levels differ due to the different electron counts. We attempted to stabilize an antiferromagnetic solution for  $\text{Co}_2\text{TiSi}$  in which the two Co atoms in the unit cell have opposite spin. We did this by performing self-consistent calculations with various initial conditions and also by performing fixed spin moment calculations with the total moment set to zero and opposite moments as the initial condition. The only solution that we were able to find was one in which the moments were zero. As mentioned the fact that moments are only stable for some arrangements means that this is not a local moment system and is instead itinerant. This itinerant nature of  $\text{Co}_2\text{TiSi}$  is consistent with the conclusions of Barth and co-workers [22,23].

However, in contrast to  $\text{Co}_2\text{TiSi}$ , fixed spin moment calculations for  $\text{Co}_2\text{MnSi}$  and  $\text{Co}_2\text{FeSi}$  with zero total moment do have spin polarized solutions. In particular with the total moment set to zero we find Mn and Fe moments opposite to the Co. This indicates stability of the Fe and Mn moments. The calculated energies as a function of spin magnetization for the three compounds are shown in Fig. 5. The corresponding moments in the transition element LAPW spheres (radius 2.3 Bohr) are shown in Fig. 6. As seen, the magnetic energy scales for  $\text{Co}_2\text{MnSi}$  and  $\text{Co}_2\text{FeSi}$  are much higher than that of  $\text{Co}_2\text{TiSi}$ . Also the minimum energies for  $\text{Co}_2\text{TiSi}$  and  $\text{Co}_2\text{MnSi}$  are at integer spin magnetization, while that of  $\text{Co}_2\text{FeSi}$  is not, in accord with the self-consistent calculations.

The individual moments show that there is practically no polarization of Ti, as expected. Importantly, the Co moments behave very differently than the Fe and Mn moments. In particular, the constraint of the fixed spin moment is achieved almost entirely through variation of the Co moments, while the Mn and Fe moments are much stiffer. This means that the Fe and Mn atoms behave as if they have local moments, while the Co backbone is itinerant in nature.

Therefore, the magnetic behavior of  $\text{Co}_2\text{MnSi}$  and  $\text{Co}_2\text{FeSi}$  can be understood in terms of local Mn or Fe moments interacting with an itinerant electron system. Interestingly, this

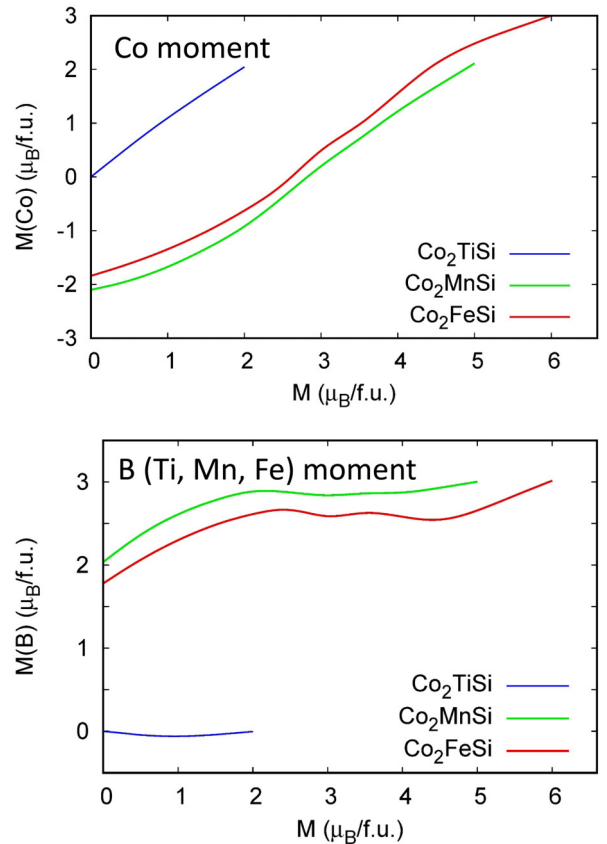


FIG. 6. Fixed spin moment moments as a function of the total moment per unit cell. The moments are per formula unit, i.e., the moment in the two Co atoms (upper panel) and in the B (Ti, Mn, or Co) atom (lower panel).

is similar to the well known spintronic material  $(\text{Ga},\text{Mn})\text{As}$ , where itinerant holes mediate interactions between Mn local moments [67]. The difference in the present case is that here the itinerant background is already an ordered ferromagnet.

#### IV. SUMMARY AND CONCLUSIONS

We report a density functional study of the ferromagnetic cobalt-based Heusler silicides, in particular  $\text{Co}_2\text{MnSi}$ ,  $\text{Co}_2\text{FeSi}$  and the parent compound  $\text{Co}_2\text{TiSi}$ . We find that  $\text{Co}_2\text{FeSi}$  is not half metallic, similar to prior standard density functional studies. However, we find nonetheless that although not a half metal, it has a very high transport spin polarization, and interestingly this is opposite to the density of states spin polarization. While this is not important for tunneling magnetoresistance devices, such as those used in read heads of hard disk technology, it is germane to other spintronic applications involving spin polarized currents. We also find that the spin excitations from our calculations, which do not yield a half-metallic state for  $\text{Co}_2\text{FeSi}$ , are nonetheless consistent with the experimental observation of a higher  $T_C$  for  $\text{Co}_2\text{FeSi}$  than for  $\text{Co}_2\text{MnSi}$ . Fixed spin moment calculations imply that the magnetic ordering can be understood in terms of local moments on Mn or Fe interacting through an

itinerant ferromagnetic background associated with the Co-Si framework of these compounds.

It is important to note that the chemistry and properties of  $\text{Co}_2\text{FeSi}$  are compatible with conventional electronics [68] and that transition metal silicides have been extensively used as electrode materials for Si devices [45]. Moreover  $\text{Co}_2\text{FeSi}$  has a cubic crystal structure. The lattice parameter is  $\sim 4\%$  larger than that of Si and is a very close match to both Ge and GaAs. These facts along with the high Curie temperature and high transport spin polarization suggest further investigations of  $\text{Co}_2\text{FeSi}$  as a spintronic material. The results also suggest additional experiments to confirm the low temperature spin magnetization of well ordered  $\text{Co}_2\text{FeSi}$ .

## ACKNOWLEDGMENTS

This work was supported by the US Department of Energy, Office of Science, Office of Basic Energy Sciences, Award Number DE-SC0019114. G.Q. is grateful for support from the China Scholarship Council (CSC). Support for work at Shanghai University was provided by the National Natural Science Foundation of China (Grants No. 51672171, No. 51861145315, and No. 51911530124), Independent Research Project of State Key Laboratory of Advanced Special Steel and Shanghai Key Laboratory of Advanced Ferrometallurgy at Shanghai University, the fund of the State Key Laboratory of Solidification Processing in NWPU (Grant No. SKLSP201703).

- [1] O. Gutfleisch, *J. Phys. D: Appl. Phys.* **33**, 157 (2000).
- [2] A. S. Sefat, R. Jin, M. A. McGuire, B. C. Sales, D. J. Singh, and D. Mandrus, *Phys. Rev. Lett.* **101**, 117004 (2008).
- [3] S. Wurmehl, G. H. Fecher, H. C. Kandpal, V. Ksenofontov, C. Felser, H. J. Lin, and J. Morais, *Phys. Rev. B* **72**, 184434 (2005).
- [4] S. Wurmehl, G. H. Fecher, H. C. Kandpal, V. Ksenofontov, and C. Felser, *Appl. Phys. Lett.* **88**, 032503 (2006).
- [5] D. Comtesse, B. Geisler, P. Entel, P. Kratzer, and L. Szunyogh, *Phys. Rev. B* **89**, 094410 (2014).
- [6] M. Jourdan, J. Minar, J. Braun, A. Kronenberg, S. Chadov, B. Balke, A. Gluskovskii, M. Kolbe, H. J. Elmers, G. Schonhense, H. Ebert, C. Felser, and M. Klau, *Nat. Commun.* **5**, 3974 (2014).
- [7] E. Sasioglu, L. M. Sandratskii, P. Bruno, and I. Galanakis, *Phys. Rev. B* **72**, 184415 (2005).
- [8] M. Meinert, C. Friedrich, G. Reiss, and S. Blugel, *Phys. Rev. B* **86**, 245115 (2012).
- [9] Z. Gersci, A. Rajanikanth, Y. K. Takahashi, K. Hono, M. Kikuchi, N. Tezuka, and K. Inomata, *Appl. Phys. Lett.* **89**, 082512 (2006).
- [10] K. Inomata, S. Okamura, A. Miyazaki, M. Kikuchi, N. Tezuka, M. Wojcik, and E. Jedryka, *J. Phys. D: Appl. Phys.* **39**, 816 (2006).
- [11] C. G. F. Blum, C. A. Jenkins, J. Barth, C. Felser, S. Wurmehl, G. Friemel, C. Hess, G. Behr, B. Buchner, A. Reller, S. Riegg, S. G. Ebbinghaus, T. Ellis, P. J. Jacobs, J. T. Kohlhepp, and H. J. M. Swagten, *Appl. Phys. Lett.* **95**, 161903 (2009).
- [12] L. Makinistian, M. M. Faiz, R. P. Panguluri, B. Balke, S. Wurmehl, C. Felser, E. A. Albanesi, A. G. Petukhov, and B. Nadgorny, *Phys. Rev. B* **87**, 220402(R) (2013).
- [13] Y. Takamura, T. Suzuki, Y. Fujino, and S. Nakagawa, *J. Appl. Phys.* **115**, 17C732 (2014).
- [14] M. Emmel, A. Alfonsov, D. Legut, A. Kehlberger, E. Vilanova, I. P. Krug, D. M. Gottlob, M. Belesi, B. Buchner, M. Klau, P. M. Oppeneer, S. Wurmehl, H. J. Elmers, and G. Jakob, *J. Magn. Magn. Mater.* **368**, 364 (2014).
- [15] W. Zhu, D. Wu, B. Zhao, Z. Zhu, X. Yang, Z. Zhang, and Q. Y. Jin, *Phys. Rev. Appl.* **8**, 034012 (2017).
- [16] W. Zhu, Z. Zhu, D. Li, G. Wu, L. Xi, Q. Y. Jin, and Z. Zhang, *J. Magn. Magn. Mater.* **479**, 179 (2019).
- [17] T. Graf, C. Felser, and S. S. P. Parkin, *Prog. Solid State Chem.* **39**, 1 (2011).
- [18] G. H. Fecher, H. C. Kandpal, S. Wurmehl, and C. Felser, *J. Appl. Phys.* **99**, 08J106 (2006).
- [19] J. Kubler, G. H. Fecher, and C. Felser, *Phys. Rev. B* **76**, 024414 (2007).
- [20] K. H. J. Buschow, P. G. van Engen, and R. Jongebreur, *J. Magn. Magn. Mater.* **38**, 1 (1983).
- [21] V. Niclescu, T. J. Burch, K. Raj, and J. I. Budnick, *J. Magn. Magn. Mater.* **5**, 60 (1977).
- [22] J. Barth, G. H. Fecher, B. Balke, T. Graf, A. Shkabko, A. Weidenkaff, P. Klaer, M. Kallmayer, H. J. Elmers, H. Yoshikawa, S. Ueda, K. Kobayashi, and C. Felser, *Philos. Trans. Roy. Soc. A* **369**, 3588 (2011).
- [23] J. Barth, G. H. Fecher, B. Balke, S. Ouardi, T. Graf, C. Felser, A. Shkabko, A. Weidenkaff, P. Klaer, H. J. Elmers, H. Yoshikawa, S. Ueda, and K. Kobayashi, *Phys. Rev. B* **81**, 064404 (2010).
- [24] P. J. Webster, *J. Phys. Chem. Sol.* **32**, 1221 (1971).
- [25] J. P. Perdew, K. Burke, and M. Ernzerhof, *Phys. Rev. Lett.* **77**, 3865 (1996).
- [26] D. J. Singh and L. Nordstrom, *Planewaves, Pseudopotentials, and the LAPW Method*, 2nd ed. (Springer, Berlin, 2006).
- [27] P. Blaha, K. Schwarz, G. K. H. Madsen, D. Kvasnicka, and J. Luitz, *WIEN2k: An Augmented Plane Wave plus Local Orbitals Program for Calculating Crystal Properties* (Technische Universität Wien, Wien, 2001).
- [28] K. Dewhurst, <http://elk.sourceforge.net/>.
- [29] H. C. Kandpal, G. H. Fecher, C. Felser, and G. Schonhense, *Phys. Rev. B* **73**, 094422 (2006).
- [30] M. Cococcioni and S. de Gironcoli, *Phys. Rev. B* **71**, 035105 (2005).
- [31] Y. Fu and D. J. Singh, *Phys. Rev. B* **100**, 045126 (2019).
- [32] K. Nawa and Y. Miura, *RSC Adv.* **9**, 30462 (2019).
- [33] P. J. Brown, K. R. A. Ziebeck, J. Desportes, and D. Givord, *J. Appl. Phys.* **55**, 1881 (1984).
- [34] H. A. Mook and J. W. Lynn, *J. Appl. Phys.* **57**, 3006 (1985).
- [35] E. Sasioglu, I. Galanakis, C. Friedrich, and S. Blugel, *Phys. Rev. B* **88**, 134402 (2013).
- [36] F. J. Dyson, *Phys. Rev.* **75**, 1736 (1949).
- [37] E. K. U. Gross and W. Kohn, *Phys. Rev. Lett.* **55**, 2850 (1985).
- [38] P. Buczek, A. Ernst, P. Bruno, and L. M. Sandratskii, *Phys. Rev. Lett.* **102**, 247206 (2009).
- [39] N. Singh, P. Elliott, T. Nautiyal, J. K. Dewhurst, and S. Sharma, *Phys. Rev. B* **99**, 035151 (2019).

- [40] V. Sharma, A. K. Solanki, and A. Kashyap, *J. Magn. Magn. Mater.* **322**, 2922 (2010).
- [41] G. K. H. Madsen and D. J. Singh, *Comput. Phys. Commun.* **175**, 67 (2006).
- [42] D. J. Singh, *J. Appl. Phys.* **79**, 4818 (1996).
- [43] B. Nadgorny, M. S. Osofsky, D. J. Singh, G. T. Woods, R. J. Soulen, Jr., M. K. Lee, S. D. Bu, and C. B. Eom, *Appl. Phys. Lett.* **82**, 427 (2003).
- [44] D. C. Worledge and T. H. Geballe, *Phys. Rev. Lett.* **85**, 5182 (2000).
- [45] J. P. Gambino and E. G. Colgan, *Mater. Chem. Phys.* **52**, 99 (1998).
- [46] A. Dahal, J. Gunasekera, L. Harringer, D. K. Singh, and D. J. Singh, *J. Alloys Compds.* **672**, 110 (2016).
- [47] Y. Wu, J. Xiang, C. Yang, W. Lu, and C. M. Lieber, *Nature (London)* **430**, 61 (2004).
- [48] M. Julliere, *Phys. Lett. A* **54**, 225 (1975).
- [49] J. S. Moodera, L. R. Kinder, T. M. Wong, and R. Meservey, *Phys. Rev. Lett.* **74**, 3273 (1995).
- [50] E. Y. Tsybal, O. N. Mryasov, and P. R. LeClair, *J. Phys.: Condens. Matter* **15**, R109 (2003).
- [51] M. J. M. de Jong and C. W. J. Beenakker, *Phys. Rev. Lett.* **74**, 1657 (1995).
- [52] R. J. Soulen, Jr., J. M. Byers, M. S. Osofsky, B. Nadgorny, T. Ambrose, S. F. Cheng, P. R. Boussard, C. T. Tanaka, J. Nowak, J. S. Moodera, A. Barry, and J. M. D. Coey, *Science* **282**, 85 (1998).
- [53] Y. Ji, G. J. Strijkers, F. Y. Yang, C. L. Chien, J. M. Byers, A. Anguelouch, G. Xiao, and A. Gupta, *Phys. Rev. Lett.* **86**, 5585 (2001).
- [54] G. E. Blonder, M. Tinkham, and T. M. Klapwijk, *Phys. Rev. B* **25**, 4515 (1982).
- [55] I. I. Mazin, A. A. Golubov, and B. Nadgorny, *J. Appl. Phys.* **89**, 7576 (2001).
- [56] E. C. Stoner, *Proc. R. Soc. Lond. Ser. A* **169**, 339 (1939).
- [57] T. Moriya and Y. Takahashi, *Ann. Rev. Mater. Sci.* **14**, 1 (1984).
- [58] E. Svanidze, J. K. Wang, T. Besara, L. Liu, Q. Huang, T. Siegrist, B. Frandsen, J. W. Lynn, A. H. Nevidomskyy, M. B. Gamza, M. C. Aronson, Y. J. Uemura, and E. Morosan, *Nat. Commun.* **6**, 7701 (2015).
- [59] H. A. Mook and D. M. Paul, *Phys. Rev. Lett.* **54**, 227 (1985).
- [60] E. E. Rodriguez, F. Poineau, A. Llobet, B. J. Kennedy, M. Avdeev, G. J. Thorogood, M. L. Carter, R. Seshadri, D. J. Singh, and A. K. Cheetham, *Phys. Rev. Lett.* **106**, 067201 (2011).
- [61] J. An, A. S. Sefat, D. J. Singh, and M. H. Du, *Phys. Rev. B* **79**, 075120 (2009).
- [62] C. J. Honer, M. J. Prosniewski, A. Putatunda, and D. J. Singh, *J. Phys.: Condens. Matter* **29**, 405501 (2017).
- [63] D. J. Singh, *Phys. Rev. B* **92**, 174403 (2015).
- [64] A. R. M. Iasir, T. Lombardi, Q. Lu, A. M. Mofrad, M. Vaninger, X. Zhang, and D. J. Singh, *Phys. Rev. B* **101**, 045107 (2020).
- [65] K. Schwarz and P. Mohn, *J. Phys. F: Metal Phys.* **14**, L129 (1984).
- [66] V. L. Moruzzi, P. M. Marcus, K. Schwarz, and P. Mohn, *Phys. Rev. B* **34**, 1784 (1986).
- [67] F. Matsukura, H. Ohno, A. Shen, and Y. Sugawara, *Phys. Rev. B* **57**, R2037 (1998).
- [68] Y. Takamura, R. Nakane, H. Munekata, and S. Sugahara, *J. Appl. Phys.* **103**, 07D719 (2008).